Structural phases arising from reconstructive and isostructural transitions in high-melting-point oxides under hydrostatic pressure: A first-principles study

Hao Tian, Xiao-Yu Kuang, Ai-Jie Mao, Yurong Yang, Changsong Xu, S. Omid Sayedaghaee, and L. Bellaiche

Novel structural phases arising from reconstructive and isostructural transitions in high-melting-point oxides under hydrostatic pressure: a first-principles study

Hao Tian,[1, 2] Xiao-Yu Kuang,[1] Ai-Jie Mao,[1, *] Yurong Yang,[2, †]
Changsong Xu,[2] S. Omid Sayedaghaee,[3] and L. Bellaiche[2, ‡]

[1] *Institute of Atomic and Molecular Physics, Sichuan University, Chengdu 610065, China*
[2] *Physics Department and Institute for Nanoscience and Engineering,*
University of Arkansas, Fayetteville, Arkansas 72701, USA
[3] *Microelectronics-Photonics Program and Physics Department,*
University of Arkansas, Fayetteville, Arkansas 72701, USA
(Dated: January 11, 2018)

High-melting-point oxides of chemical formula ABO_3, with A = Ca, Sr, Ba and B = Zr, Hf, are investigated as a function of hydrostatic pressure up to 200 GPa, by combining first-principles calculations with a particle swarm optimization method. Ca- and Sr-based systems (1) first undergo a reconstructive phase transition from a perovskite state to a novel structure that belongs to the post-post-perovskite family; and (2) then experience an isostructural transition to a second, also new post-post-perovskite state at higher pressure, via the sudden formation of a specific out-of-plane B-O bond. In contrast, the studied Ba-compounds evolve from a perovskite phase to a third novel post-post-perovskite structure, via another reconstructive phase transition. Original characteristics of these three different post-post-perovskite states are emphasized. Unusual electronic properties, including significant piezochromic effects and an insulator-metal transition, are also reported and explained.

PACS numbers: 61.50.Ks, 64.70.K-, 81.30.-t

Zirconate and hafnate oxides, with a perovskite structure, are intensively studied for their use in protonic/ionic conducting and resistance switching applications [1–6]. In addition to undergoing a series of phase transitions with temperature [7–9], these compounds have a rather high melting point (over 2880 K for $SrZrO_3$ and $SrHfO_3$ [7]) that makes them suitable for use in high-temperature applications such as fuel cells, steam electrolysis, and hydrogen gas sensors [10, 11]. Moreover, barium zirconate and barium hafnate perovskite oxides also possess a good thermodynamic stability, low reactivity and a large lattice constant, which render them suitable substrates for the synthesis of high-temperature superconductors or for inducing large epitaxial tensile strain in perovskite films [12, 13].

Interestingly, applying hydrostatic pressure is an efficient way to achieve novel properties due to its influence on crystal structure, electronic orbitals, chemical bonding, etc. Many exotic materials have been formed under pressure, such as compressed H_3S exhibiting high-temperature superconductivity [14–16], diamond-like BC_5 possessing Vickers hardness $H_V = 71$ GPa [17], and hydrogen-rich metal hydrides RhH_2 that are promising for hydrogen storage [18]. ABO_3 and ABF_3 materials were also found and/or predicted to possess crystal structures that differ from perovskite, when placed under hydrostatic pressure, as, e.g., evidenced by (1) the discovery of the so-called post-perovskite phase of $MgSiO_3$ in the lowermost layer of the Earth's mantle [19, 20]; (2) the facts that $NaMgF_3$ and $CaTiO_3$ can further transform from a post-perovskite phase to a post-post-perovskite phase under higher pressure [21]; and (3) the pressure-induced post-post-perovskite structure of $RMnO_3$ (where R is a rare-earth ion) adopting a novel polar and magnetic- and therefore multiferroic- phase, as originating from novel energetic couplings between the electrical polarization and pseudo Jahn-Teller effects [22].

Based on the interest that high-melting-point oxides exercise and these recent findings on high-pressure-induced novel structures in other perovskites, it is legitimate to wonder if ABO_3 materials, with A = Ca, Sr, Ba, and B = Zr, Hf, can also adopt new phases when subject to pressure. If so, revealing and understanding the structural mechanism(s) yielding such (hypothetical) new phases would also be of obvious importance. The main goal of this manuscript is to reveal the prediction of three novel pressure-induced phases that can all be considered to belong to the post-post-perovskite family (therefore broadening such family via the original ways that oxygen polyhedra interconnect to each other to form a network) in these high-melting-point oxides, as a result of either reconstructive or isostructural phase transitions. We also found that such phases can have a large variation of their electronic band gap as a function of pressure (that is they exhibit significant piezochromic effects), even resulting in a pressure-induced insulator-to-metallic transition.

To explore possible crystal structures that are stable under hydrostatic pressures, we performed simulations of these ABO_3 systems under 50, 100, and 150 GPa, as well as ambient pressure, using CALYPSO (crystal structure analysis by particle swarm optimization) [23, 24].
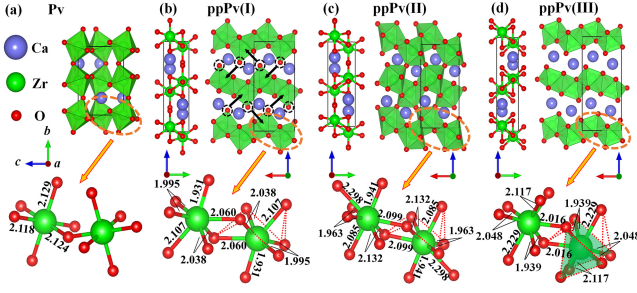
FIG. 1. Schematization of (a) the Pv-*Pnma* (0 GPa), (b) ppPv-*Pnma*(I) (130 GPa), (c) ppPv-*Pnma*(II) (140 GPa), and (d) ppPv-*Pnma*(III) (140 GPa) states in CaZrO₃ under pressure. The bottom figures depict two local adjacent polyhedral in these structures, with the red dotted lines indicating shared common edges and the translucent green planes representing shared common faces.

Computations for the lowest-energy candidate structures are then conducted, for any pressure ranging between 0 and 200 GPa, using the density functional theory (DFT) [25] within the Perdew-Burke-Emzerhof (PBE) generalized gradient approximation (GGA) functional [26], as implemented in the Vienna *ab initio* Simulation Package (VASP) [27]. The Supplemental Materials [28–33] provide more details about our computations, and also show that the use of the so-called PBEsol functional [34] yields similar results. Note also that the PBE functional has been demonstrated to provide accurate results at high pressure, in, e.g., superconducting hydrogen sulfide and the post-perovskite phase of MgSiO₃ [14–16, 19, 20].

Let us start by focusing on CaZrO₃ (CZO). As consistent with previous works [35–37], CZO is found to exhibit the perovskite (Pv) structure, with the orthorhombic *Pnma* space group, as its ground state. This phase is denoted as Pv-*Pnma* and shown in Fig. 1a. One can, e.g., see that, as typical of perovskites, any oxygen octahedron shares a corner with a neighboring octahedron to form a three-dimensional network. The predicted lattice parameters of the Pv-*Pnma* ground state of CZO are a = 5.828 Å, b = 8.094 Å, and c = 5.632 Å, which is in rather good agreement (i.e., typically within 1%) with the measurements of Ref. [36]. Figure 2a reports the enthalpy H = E + PV (where E is the total internal energy, P is the hydrostatic pressure, and V is the volume) as a function of pressure for the different phases that the CALYPSO software [23, 24] determined in CZO. In this figure, the enthalpy of the perovskite phase adopting the orthorhombic *Cmcm* phase (to be coined Pv-*Cmcm*) is set to be zero for any pressure. Figure 2a indicates that, up to 10 GPa, Pv-*Pnma* remains the most stable state since it has the lowest enthalpy (the Pv-*Cmcm* phase of CZO, that has been mentioned in Ref. [35], is therefore of higher enthalpy). In this stable Pv-*Pnma* phase, there are three doubly degenerate Zr-O nearest neighbor bonds, that are all very close to each other and that de-

crease with pressure, as indicated in the bottom of Fig. 1a and as shown in Fig. 2c. The resulting coordination around each Zr ion is therefore equal to 6 in Pv-*Pnma*. When the pressure reaches about 10 GPa, a first-order transition occurs from Pv-*Pnma* to the phase displayed in Fig. 1b. Such phase also possesses the orthorhombic *Pnma* space group, but adopts a crystal structure that differs from perovskite. As shown in Figs 1b and 2b, such crystal structure is such as (i) any two adjacent oxygen polyhedra share common edges, leading to a network of connected polyhedra within any c plane; and (ii) its c-axis is strongly elongated, while its b-axis is significantly shortened, with respect to the a-axis. Such crystal structure can therefore be considered to be what was termed as a post-post-perovskite (ppPv) structure in Ref. [18]. The resulting *Pnma* state of CZO within this post-post-perovskite (ppPv) structure is denoted as ppPv-*Pnma*(I). In our discovered ppPv-*Pnma*(I) state, any oxygen polyhedron is connected with six other polyhedra within any given c-plane via six edge sharings. Such features make ppPv-*Pnma*(I) differ from the post-post-perovskite structure of Ref. [21] and shown in Fig. S1, for which any oxygen polyhedron is connected with four oxygen polyhedra via four edge sharings. Post-post-perovskite phases can therefore be diverse. In fact, other post-post-perovskite states to be discussed below, and to be denoted as ppPv-*Pnma*(II) and ppPv-*Pnma*(III), are also different from that of Ref. [21], therefore confirming such diversity as well as the novel character of various phases reported in the present work. Furthermore, Figure 2b indicates that, at the Pv-*Pnma*-to-ppPv-*Pnma*(I) transition of about 10 GPa in CZO, the lattice parameter a remains nearly identical while the b and c parameters suddenly experience a large decrease by 41.2% and increase by 56.4%, respectively, which results in large volume collapse ($\sim$ 7.7%) that is representative of a strong first-order transition. The coordination around each Zr ion is increased from 6 to 7 at that transition since there are two doubly degenerate and three non-degenerate different Zr-O bonds in ppPv-*Pnma*(I), as revealed by the bottom part of Fig. 1b. At around 10GPa, some of these seven bonds of ppPv-*Pnma*(I) reach values as large as 2.3 Å, while all the six bonds of Pv-*Pnma* are less than 2.1 Å. Such change in bonding, as well as the dramatic difference in structures between Pv-*Pnma* phase and ppPv-*Pnma*(I) state, implies that Pv-*Pnma*-to-ppPv-*Pnma*(I) can be considered to a be a textbook example of *reconstructive* phase transitions [38] (that are first-order in nature [39]). Note also that all the seven short Zr-O bonds of ppPv-*Pnma*(I) decreases with pressure, as indicated in Fig. 2c.

Moreover, there is another distance between Zr and O ions that is much larger than these seven bonds in ppPv-*Pnma*(I). This distance is shown in Fig. 1b, via black arrows, and is, e.g., close to 2.94 Å at about 130GPa while the largest of these seven bonds is less than 2.1 Å at this pressure (see Fig. 2c). Remarkably, this dis-
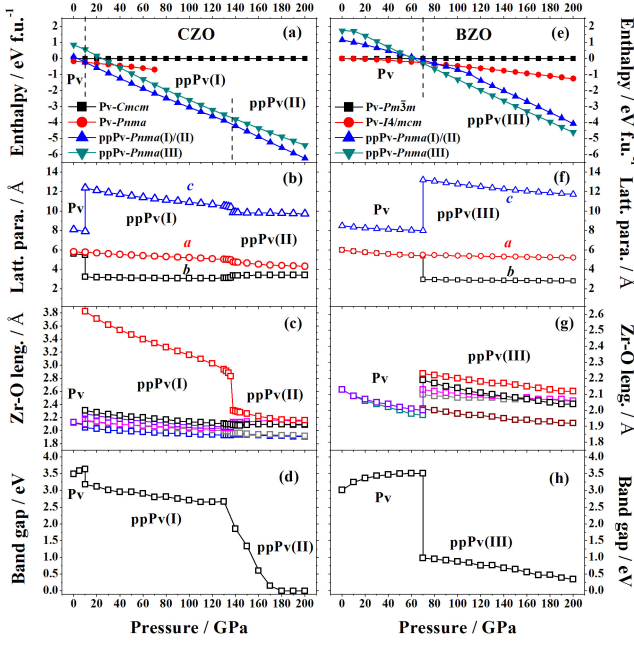
FIG. 2. Predicted (a) enthalpy, (b) lattice parameters, (c) the short Zr-O bonds lengths, and (d) electronic band gap versus hydrostatic pressure for low-in-enthalpy phases in CaZrO$_3$. Note that the enthalpy of the Pv-$Cmcm$ phase has been set to be zero for any pressure in Panel a; Panel (e-h): Same as Panels (a-d), respectively, but for BaZrO$_3$ and with the enthalpy of the Pv-$Pm\bar{3}m$ phase having been set to be zero for any pressure in Panel e.

the case of ppPv-$Pnma$(I). Any oxygen polyhedron in ppPv-$Pnma$(II) is now linked with 8 other polyhedra via 6 edge sharings in a c-plane and 2 corner sharings out of this c-plane. Such features emphasize the fact that ppPv-$Pnma$(II) is structurally different from ppPv-$Pnma$(I) and from the post-post-perosvkite phase of Ref. [21]

There is another post-post-perosvkite state, to be denoted as ppPv-$Pnma$(III), that is found in our simulations of CZO. It is shown in Fig. 1d, and is such as that any oxygen polyhedron is connected to 6 neighboring polyhedra – via 4 typical edge sharings and 2 face sharings (with each face sharing being formed by 3 triangular edge sharings). However, as indicated in Fig. 2b, such ppPv-$Pnma$(III) state has an enthalpy that is always larger than the ones of ppPv-$Pnma$(I) and ppPv-$Pnma$(II) in CZO, which implies that ppPv-$Pnma$(III) is never the equilibrium phase of CZO for any pressure. As we are going to see below, this is not the case for BaZrO$_3$ (BZO).

However, before that, let us demonstrate that structural changes can affect other physical properties, as evidenced by, e.g., the variation of the electronic band gap of CZO *versus* pressure displayed in Fig. 2d. In particular, the ppPv-$Pnma$(II) phase of CZO possesses a (direct) electronic band gap that varies from 1.80 to about 0 eV when the pressure increases from about 140 to 180 GPa. In other words, CZO in its ppPv-$Pnma$(II) phase possesses rather large *piezochromic* effects – i.e., change of color under pressure – and can even undergo an insulator-to-metallic transition [41]. Such striking effect can be understood thanks to Figs. 3 that report the total and projected local density of states of CZO between 130 and 180 GPa, as well as the corresponding charge density integrated over all the conduction states having an energy being within 0.3 eV of the conduction band minimum. Such figures reveal that the isostructural transition from ppPv-$Pnma$(I)-to-ppPv-$Pnma$(II) leads to the formation of (empty) antibonding orbitals between two Zr ions (with these two Zr ions being each involved in the aforementioned newly formed Zr-O bonds). Such antibonding results in a broadening of the Zr-4d dominated lowest conduction band and concomitant shift of the conduction band minimum energy towards the (oxygen-2p dominated) valence band maximum as pressure increases (since the distance between these two antibonded Zr ions decrease with pressure, as shown in Fig. S6 of the Supplemental Material). As a result, the band gap decreases with pressure between 140 and 180 GPa within the ppPv-$Pnma$(II) phase. Note also that pressure-induced insulator-to-metal transitions have also been reported in other systems, but when no structural phase transition occurs [42].

Let us now pay attention to BZO. At ambient pressure and room temperature, BZO is known to possess a high symmetric cubic perovskite structure having the $Pm\bar{3}m$

tance suddenly decreases from about 2.8 Å to about 2.3 Å at $\sim$ 138 GPa, leading to another first-order transition in which the resulting phase has now a coordination of 8 (two doubly degenerate and four non-degenerate Zr-O chemical bonds). This resulting phase not only retains the same $Pnma$ space group but also continues to adopt the post-post-perovskite structure (characterized, e.g., by any two neighboring polyhedra sharing oxygen edges within c-planes), as similar to ppPv-$Pnma$(I). We will thus denote such new phase as ppPv-$Pnma$(II). Interestingly, all the atoms in ppPv-$Pnma$(II) occupy the same types of Wyckoff positions than in ppPv-$Pnma$(I), as detailed in Table S1 of the Supplemental Materials, while the ppPv-$Pnma$(I)-to-ppPv-$Pnma$(II) transition is accompanied by a sudden change in lattice parameters by less than 6% (see Fig. 2b) which generates a reduction in volume of $\sim$ 2.9%. The ppPv-$Pnma$(I)-to-ppPv-$Pnma$(II) is therefore an example of a (first-order) *isostructural* phase transitions [40], which are rather rare in nature. Note that the new atomic bond formed by the shortening of the aforementioned specific Zr-O distance at the ppPv-$Pnma$(I)-to-ppPv-$Pnma$(II) transition can be clearly seen in Fig. S2 of the Supplemental Materials. Such new bond allows oxygen polyhedra of different c-planes to be now connected to each other via corner-sharing in ppPv-$Pnma$(II), which contrasts with

space group [43]. Moreover, some first-principles simulations (therefore conducted at 0K) further predict that BZO can, in fact, exhibit small antiphase tilting of the oxygen octahedra in its ground state [44, 45]. However, such low-temperature tiltings have also been suggested to be suppressed by quantum effects [44]. Our simulations of Fig. 2e are consistent with all these previous works since we found that two different perovskite structures have the lowest and close enthalpies from 0 GPa to about 20 GPa, namely the aforementioned cubic $Pm\bar{3}m$ phase (to be denoted here as Pv-$Pm\bar{3}m$), and the tetragonal $I4/mcm$ state (to be referred to as Pv-$I4/mcm$) that has antiphase tilting of its oxygen octahedra about the [001] direction. The angle of these tiltings in Pv-$I4/mcm$ is equal to 3.4° at 0 Ga and increases up to 8.5° for the pressure of 20 GPa. It is only above 20 GPa and up to about 70 GPa that Pv-$I4/mcm$ has an enthalpy lower by more than 35 meV/5-atom from that of Pv-$Pm\bar{3}m$ (with this difference increasing with pressure), which is in-line with the phase transition from cubic Pv-$Pm\bar{3}m$ to Pv-$I4/mcm$ that has been observed at 17.2GPa in BZO at room temperature [46]. Unlike in CZO, the perovskite $Pnma$ phase is never the equilibrium state of BZO at any pressure. Another major difference between CZO and BZO is that this latter transforms at higher pressure towards a post-post-perovskite structure that is neither ppPv-$Pnma$(I) nor ppPv-$Pnma$(II), but rather to what we called ppPv-$Pnma$(III) and that is depicted in Fig. 1d. The transition from Pv-$I4/mcm$ to ppPv-$Pnma$(III) occurs at about 70 GPa, as revealed by Fig. 2e. Note that this latter figure also indicates that ppPv-$Pnma$(III) possesses a higher enthalpy than ppPv-$Pnma$(I) for pressures ranging from 0 to 50GPa (for which the ground state is perovskite), with this hierarchy between the enthalpies of these two post-post-perovskites phases reverting itself above 50GPa. Moreover, Fig. 2f shows that the Pv-$I4/mcm$-to-ppPv-$Pnma$(III) transition is accompanied by a sudden decrease of the b lattice parameter by a factor of about 0.55 and an enhancement of about 1.65 times for c, while a appears to continuously evolve during the transition. Such evolutions result in a 7.9% volume collapse at this transition. Furthermore, the coordination around each Zr ion increases from 6 (arising from one doubly degenerate Zr-O bond and another quadruply degenerate Zr-O bond) to 8 (three doubly degenerate and two non-degenerate Zr-O bonds) at the Pv-$I4/mcm$-to-ppPv-$Pnma$(III) transition, as shown in Fig. 2g. These changes in volume and bonding are representative of another first-order reconstructive phase (note that Fig. 2h reveals that BZO exhibits a sudden decrease of its band gap by about 2.5 eV at this reconstructive transition, as also further detailed in Fig. S7. of the Supplemental Material). It is also worthwhile to realize that, unlike in CZO, there is no predicted phase transition between two different post-post-perovskite states in BZO until reaching the highest investigated pressure of 200GPa, that

is this Ba-system remains in the ppPv-$Pnma$(III) phase from 70 to 200GPa.

Let us now provide more information about ppPv-$Pnma$(III). As its name indicates, its space group is also orthorhombic $Pnma$ and it also possesses edge-sharing oxygen polyhedra that are characteristic of post-post-perovskite structures (see Fig. 1d). One main distinction between ppPv-$Pnma$(III) and the other two post-post-perovskite ppPv-$Pnma$(I) and ppPv-$Pnma$(II) structures is that the Wycoff y-coordinates of the Ca ion and of one oxygen ion (the one denoted as O3 in Table S1) are both equal to 0.75, while they are 0.25 in ppPv-$Pnma$(I) and ppPv-$Pnma$(II). Such changes naturally affect, e.g., Ca-Zr bonds: ppPv-$Pnma$(III) has three non-degenerate Ca-Zr (shortest) bonds to be compared with five (two doubly degenerate and one non-degenerate) Ca-Zr bonds in both ppPv(I) and ppPv(II). The patterns formed by these Ca-Zr bonds in these three post-post-perovskite phases are shown in Fig. S4 of the Supplementary Materials.

In addition to CZO and BZO, we also investigated CaHfO$_3$, SrZrO$_3$, SrHfO$_3$ and BaHfO$_3$, under pressures up to 200GPa. As indicated in the Supplemental materials, CaHfO$_3$, SrZrO$_3$ and SrHfO$_3$ *qualitatively* behave
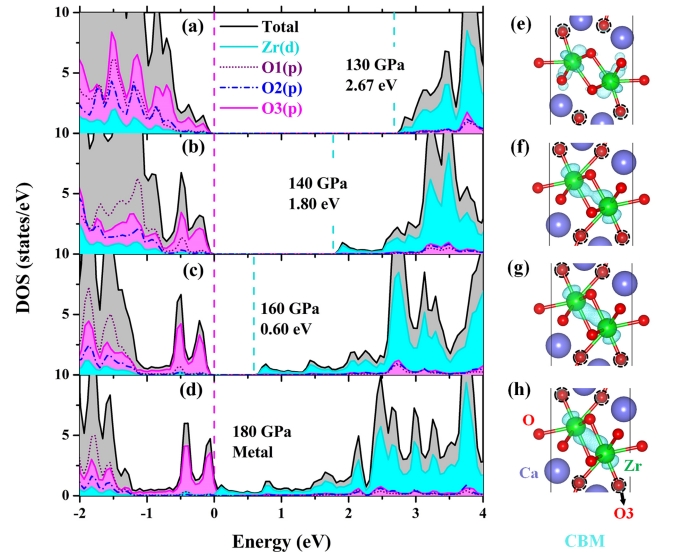

FIG. 3. (a-d) Total and projected density of states of the equilibrium ppPv(I)/(II)-Pnma structure for CaZrO3 for 130 GPa (corresponding to ppPv(I)-Pnma), as well as for 140, 160 and 180 GPa (all associated with ppPv(II)-Pnma). The magenta dotted vertical lines are set as the Fermi level, that is at the valence-band maximum (VBM). The cyan dotted vertical lines are set at the conduction-band minimum (CBM). (e-h) The corresponding charge density integrated over all the conduction states having an energy being within 0.3 eV of the conduction band minimum.The band gap is direct at the zone center. O1, O2 and O3 oxygens are the types of oxygen ions indicated in Table S1 of the Supplemental Material. In particular, each O3 ion forms a new bond with a Zr ion in ppPv(II)-Pnma, as depicted in Panels f-h. Such O3 ions are circled around in Panels e-h.

as CZO when under pressure, since (1) their adopted state at small pressures crystallizes in Pv-*Pnma*, as consistent with experiments [8, 9]; (2) they then undergo a phase transition towards ppPv-*Pnma*(I) state; (3) finally experience the isostructural ppPv-*Pnma*(I)-to-ppPv-*Pnma*(II) transition at higher pressure; and (4) possess similar *piezochromic* effects in their ppPv-*Pnma*(II) phase. Figure S3 of the Supplemental Materials also indicate that BaHfO$_3$ qualitatively behaves as BZO since its ground state is perovskite at low pressure (it is Pv-$Pm\bar{3}m$, as consistent with measurements [47, 48]), then transforms into Pv-$I4/mcm$ phase at about 10 GPa and into ppPv-*Pnma*(III) at about 90 GPa, and remains in this post-post-perovskite state up to 200GPa. Note that the difference in post-post-perovskite types of phase, as well as the two different slopes of the volume collapse-versus-critical pressure, shown in Fig. S8 of the Supplemental Material, definitely indicate that two classes of materials should be distinguished for these high-melting-point oxides: one that gathers CaZrO$_3$, CaHfO$_3$, SrZrO$_3$ and SrHfO$_3$ and another one formed by the Ba-based BaZrO$_3$ and BaHfO$_3$ compounds.

In summary, we combined a particle swarm optimization method and first-principles calculations to reveal pressure-induced structural changes in ABO$_3$ compounds with A = Ca, Sr, Ba and B = Zr, Hf. All these high-melting-point oxides are predicted to undertake a first-order reconstructive phase transition from a perovskite to a post-post-perovskite structure, that is ppPv-*Pnma*(I) in case of the Ca- and Sr-based materials *versus* ppPv-*Pnma*(III) for the Ba-systems. The experimental confirmation of the existence of these reconstructive phase transitions likely requires laser heating under pressure [49–51]. The difference between these two classes of materials is further emphasized by the fact that CaZrO$_3$, CaHfO$_3$, SrZrO$_3$ and SrHfO$_3$, unlike BaZrO$_3$ and BaHfO$_3$, further undergo an isostructural transition from ppPv-*Pnma*(I)-to-ppPv-*Pnma*(II), when the hydrostatic pressure is increased. Such latter transition is associated with the sudden formation of an out-of-plane Zr-O/Hf-O bond. Other striking structural data of ppPv-*Pnma*(I), ppPv-*Pnma*(II) and ppPv-*Pnma*(III), such as the different ways that oxygen polyhedral interconnect to each other to generate original networks, are discussed. Such structural changes are further demonstrated to generate striking physical phenomena, such as significant *piezochromic* effects in CZO, CaHfO$_3$, SrZrO$_3$ and SrHfO$_3$. We thus hope that the present study broadens the general and important fields of, e.g., phase transitions and crystallography, and will encourage scientists to observe such effects in high-melting-point oxides as well as in other systems.

————

* scu_mij@126.com(A.-J. Mao)
† yyrwater@uark.edu(Y. Yang)
‡ laurent@uark.edu(L. Bellaiche)

[1] S. C. Hwang and G. M. Choi, Solid State Ionics **179**, 1042 (2008).
[2] R. B. Cervera, Y. Oyama, S. Miyoshi, I. Oikawa, H. Takamura, and S. Yamaguchi, Solid State Ionics **264**, 1 (2014).
[3] L. Weston, A. Janotti, X. Cui, C. Stampfl, and C. Van de Walle, Phys. Chem. Chem. Phys. **19**, 11485 (2017).
[4] S. Lee, W. Zhang, F. Khatkhatay, Q. Jia, H. Wang, and J. L. MacManusDriscoll, Adv. Funct. Mater. **25**, 4328 (2015).
[5] M.-H. Lin, M.-C. Wu, C.-Y. Huang, C.-H. Lin, and T.-Y. Tseng, J. Phys. D: Appl. Phys. **43**, 295404 (2010).
[6] Y. Ding, X. Xu, A. Bhalla, X. Yang, J. Chen, and C. Chen, RSC Adv. **6**, 60074 (2016).
[7] S. Yamanaka, K. Kurosaki, T. Oyama, H. Muta, M. Uno, T. Matsuda, and S. Kobayashi, J. Am. Ceram. Soc. **88**, 1496 (2005).
[8] B. J. Kennedy, C. J. Howard, and B. C. Chakoumakos, Phys. Rev. B **59**, 4023 (1999).
[9] B. J. Kennedy, C. J. Howard, and B. C. Chakoumakos, Phys. Rev. B **60**, 2972 (1999).
[10] H. Iwahara, Y. Asakura, K. Katahira, and M. Tanaka, Solid State Ionics **168**, 299 (2004).
[11] H. Iwahara, T. Yajima, T. Hibino, K. Ozaki, and H. Suzuki, Solid State Ionics **61**, 65 (1993).
[12] R. Liang, D. Bonn, and W. Hardy, Physica C **304**, 105 (1998).
[13] M. Kim, J. Ihm, and S. B. Chung, Phys. Rev. B **94**, 115431 (2016).
[14] D. Duan, X. Huang, F. Tian, D. Li, H. Yu, Y. Liu, Y. Ma, B. Liu, and T. Cui, Physical Review B **91**, 180502 (2015).
[15] M. Einaga, M. Sakata, T. Ishikawa, K. Shimizu, M. I. Eremets, A. P. Drozdov, I. A. Troyan, N. Hirao, and Y. Ohishi, Nature physics **12**, 835 (2016).
[16] A. Drozdov, M. Eremets, I. Troyan, V. Ksenofontov, and S. Shylin, Nature **525**, 73 (2015).
[17] V. L. Solozhenko, O. O. Kurakevych, D. Andrault, Y. Le Godec, and M. Mezouar, Phys. Rev. Lett. **102**, 015506 (2009).
[18] B. Li, Y. Ding, D. Y. Kim, R. Ahuja, G. Zou, and H.-K. Mao, Proceedings of the National Academy of Sciences **108**, 18618 (2011).
[19] A. R. Oganov and S. Ono, Nature **430**, 445 (2004).
[20] A. R. Oganov, R. Martok, A. Laio, P. Raiteri, and M. Parrinello, Nature **438**, 1142 (2005).
[21] C. Xu, B. Xu, Y. Yang, H. Dong, A. R. Oganov, S. Wang, W. Duan, B. Gu, and L. Bellaiche, Phys. Rev. B **91**, 020101 (2015).
[22] C. Xu, Y. Li, B. Xu, J. iguez, W. Duan, and L. Bellaiche, Adv. Funct. Mater. **27**, 1604513 (2017).

[23] Y. Wang, J. Lv, L. Zhu, and Y. Ma, Phys. Rev. B **82**, 094116 (2010).

[24] Y. Wang, J. Lv, L. Zhu, and Y. Ma, Comput. Phys. Commun. **183**, 2063 (2012).

[25] W. Kohn and L. J. Sham, Phys. Rev. **140**, A1133 (1965).

[26] J. P. Perdew, K. Burke, and M. Ernzerhof, Phys. Rev. Lett. **77**, 3865 (1996).

[27] G. Kresse and J. Furthmller, Phys. Rev. B **54**, 11169 (1996).

[28] See Supplemental Material at [URL will be inserted by publisher] for details about the methods used, as well as additional information.

[29] C. Lu, M. Miao, and Y. Ma, J. Am. Chem. Soc. **135**, 14167 (2013).

[30] D. Die, B.-X. Zheng, L.-Q. Zhao, Q.-W. Zhu, and Z.-Q. Zhao, Sci. Rep. **6** (2016).

[31] C. Zhang, X. Kuang, Y. Jin, C. Lu, D. Zhou, P. Li, G. Bao, and A. Hermann, ACS Appl. Mater. Interfaces **7**, 26776 (2015).

[32] H. T. Stokes and D. M. Hatch, J. Appl. Crystallogr. **38**, 237 (2005).

[33] V. M. Goldschmidt, Naturwissenschaften **14**, 477 (1926).

[34] J. P. Perdew, A. Ruzsinszky, G. I. Csonka, O. A. Vydrov, G. E. Scuseria, L. A. Constantin, X. Zhou, and K. Burke, Phys. Rev. Lett. **100**, 136406 (2008).

[35] A. Kersch and D. Fischer, J. Appl. Phys. **106**, 014105 (2009).

[36] H. Koopmans, G. Van De Velde, and P. Gellings, Acta Crystallogr., Sect. C: Cryst. Struct. Commun. **39**, 1323 (1983).

[37] X. Yang, Q. Li, R. Liu, B. Liu, S. Jiang, K. Yang, J. Liu, Z. Chen, B. Zou, and T. Cui, CrystEngComm **16**, 4441 (2014).

[38] V. Dmitriev, S. Rochal, Y. M. Gufan, and P. Toledano,

[39] Phys. Rev. Lett. **60**, 1958 (1988).

[39] K. Binder, Rep. Prog. Phys. **50**, 783 (1987).

[40] M. Barma, T. Kaplan, and S. Mahanti, Phys. Lett. A **57**, 168 (1976).

[41] Note that our DFT results should provide accurate change of band-gap *versus* pressure but may need to be corrected for the value of the band gap at a specific pressure, because of the typical underestimation of this physical electronic quantity by DFT technique.

[42] A. Gaul, Q. Peng, D. J. Singh, G. Ramanath, and T. Borca-Tasciuc, Phys. Chem. Chem. Phys. **19**, 12784 (2017).

[43] M. Mathews, E. Mirza, and A. Momin, J. Mater. Sci. Lett. **10**, 305 (1991).

[44] A. Akbarzadeh, I. Kornev, C. Malibert, L. Bellaiche, and J. Kiat, Phys. Rev. B **72**, 205104 (2005).

[45] J. W. Bennett, I. Grinberg, and A. M. Rappe, Phys. Rev. B **73**, 180102 (2006).

[46] X. Yang, Q. Li, R. Liu, B. Liu, H. Zhang, S. Jiang, J. Liu, B. Zou, T. Cui, and B. Liu, J. Appl. Phys. **115**, 124907 (2014).

[47] A. L. Garci, P. de la Presa, and A. Rodriguez, Phys. Rev. B **44**, 9708 (1991).

[48] W. H. Payne and V. J. Tennery, J. Am. Ceram. Soc. **48**, 413 (1965).

[49] C. D. Martin, W. A. Crichton, H. Liu, V. Prakapenka, J. Chen, and J. B. Parise, Am. Mineral. **91**, 1703 (2006).

[50] C. D. Martin, W. A. Crichton, H. Liu, V. Prakapenka, J. Chen, and J. B. Parise, Geophys. Res. Lett. **33** (2006).

[51] X. Wu, J.-F. Lin, P. Kaercher, Z. Mao, J. Liu, H.-R. Wenk, and V. B. Prakapenka, Nat. Commun. **8**, 14669 (2017) .